Forest Ecology and Management 551 (2024) 121529

Contents lists available at ScienceDirect

Forest Ecology and Management

journal homepage: www.elsevier.com/locate/foreco

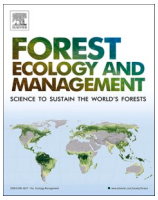

Impact of rainfall and vapor pressure deficit on latewood growth and water stress in Douglas-fir in a Mediterranean climate

Karla M. Jarecke [a,*], Kevin D. Bladon [a,b], Frederick C. Meinzer [c], Steven M. Wondzell [c]

[a] Oregon State University, Department of Forest Ecosystems and Society, Corvallis, OR 97331, USA
[b] Oregon State University, Department of Forest Engineering, Resources, and Management, Corvallis, OR 97331, USA
[c] US Forest Service, Pacific Northwest Research Station, Corvallis, OR 97331, USA

ARTICLE INFO

Keywords:
Douglas-fir
Tree rings
Carbon isotope signature
Rainfall
Vapor pressure deficit

ABSTRACT

Both elevated temperature and reduced precipitation have been related to growth declines in Douglas-fir (*Pseudotsuga menziesii*) in the northwest U.S. However, the impact of high vapor pressure deficit (VPD) on Douglas-fir growth and physiological stress is not fully understood. We investigated how inter- and intra-annual rainfall and VPD correlated to the radial growth and carbon isotope signature ($\delta^{13}C$) of latewood for ~ 50-year-old Douglas-fir trees in the western Cascade Mountains in Oregon. Latewood $\delta^{13}C$ reflects variation in stomatal restriction of photosynthetic gas exchange and, therefore, was used as a proxy for the relative degree of physiological water stress. We cored three trees at each of nine sampling sites ($n = 27$ trees) and used a moving window analysis to test the period of the year in which VPD and rainfall best predicted mean latewood radial growth and $\delta^{13}C$. Latewood growth, measured as the basal area increment, was more sensitive to daytime VPD than the timing and amounts of rainfall, especially in early summer. In contrast, $\delta^{13}C$ was equally sensitive to the average daytime VPD and total rainfall during spring and summer. We used the results of the moving window analysis in a linear mixed effects model to test how the effect of VPD and rainfall on yearly latewood growth and $\delta^{13}C$ differed among our nine sites. We found no evidence for statistical differences in the effects of VPD and rainfall on growth ($p = 0.93$ and $p = 0.91$) or $\delta^{13}C$ ($p = 0.31$ and $p = 0.81$) among our nine sites. However, the marginal effects of VPD on latewood growth at each site were weakly related to soil moisture deficits at 100 cm suggesting that site-to-site differences in soil moisture availability may be important in buffering the negative effects of seasonal aridity on growth. In contrast, there was no evidence that soil moisture differences among sites influenced the marginal effects of VPD on latewood $\delta^{13}C$. We conclude that increases in VPD during summer are likely to reduce latewood growth and increase water stress in Douglas-fir in the Pacific Northwest region. However, more research is needed to better understand the magnitude of this effect across sites with variable subsurface water storage and microclimate.

1. Introduction

Increased atmospheric vapor pressure deficit (VPD), accompanied by more severe drought, is likely to impact forest productivity in the coming century (Ficklin and Novick, 2017; Novick et al., 2016; Sanginés de Cárcer et al., 2018; Sulman et al., 2016; Yuan et al., 2019). The water potential gradient along the soil–plant-atmosphere continuum is strongly influenced by both the atmospheric demand for water and the availability of soil moisture. While high VPD is commonly associated with periods of declining soil moisture in Mediterranean climates, sustained increases in atmospheric VPD can lead to considerable reductions in stomatal conductance and photosynthesis even in the presence of sufficient soil moisture (Fang et al., 2021; Fu et al., 2022; Jarecke et al., 2023; Jiang et al., 2019; Ruehr et al., 2014). High VPD conditions can also increase the potential for hydraulic failure along the soil-to-leaf continuum (Grossiord et al., 2020), reduce tree growth rates (Restaino et al., 2016; Williams et al., 2013), and increase rates of tree mortality (Allen et al., 2015; Breshears et al., 2013).

In the northwest U.S., conifer species are expected to be increasingly vulnerable to rising VPD and soil water stress, particularly during the warm and dry periods of the year (Beedlow et al., 2013). Extensive research using dendrochronology techniques has assessed the

* Corresponding author at: Wilkinson Hall 251, 2601 SW Orchard Avenue, Corvallis, OR 97331, USA.
E-mail address: karla.jarecke@oregonstate.edu (K.M. Jarecke).

https://doi.org/10.1016/j.foreco.2023.121529
Received 12 September 2023; Received in revised form 23 October 2023; Accepted 24 October 2023

vulnerability and water stress experienced by conifers. For example, variability in the annual tree ring width has been used to understand the environmental conditions that impact a given species' growth across regional climates (e.g., interior vs. coastal) and altitudes (Chen et al., 2010; Lo et al., 2010). Previous research indicates that annual growth of inland Douglas-fir trees was positively correlated with winter and spring temperatures (Case and Peterson, 2005) as well as spring and summer rainfall (Levesque et al., 2013; Littell et al., 2008). Conversely, Douglas-fir growth was negatively correlated with summer temperature (Beedlow et al., 2013; Lo et al., 2010). In contrast, the growth of Douglas-fir trees at lower elevations or in coastal regions were most sensitive to conditions during summer, with increased growth observed in cooler and wetter summers (Griesbauer and Green, 2010; Little et al., 1995; Zhang and Hebda, 2004). It is important to note that the development of earlywood and latewood within annual growth rings may reflect environmental conditions over different periods of the year (Levesque et al., 2013). Furthermore, emerging evidence suggests that while tree ring width may be more sensitive to climate variability during the phase of cell enlargement, stable carbon isotope composition of cellulose may be more sensitive to climate variability during cell wall thickening (Belmecheri et al., 2018).

The stable carbon isotope composition of cellulose, known as $\delta^{13}C$, represents the ratio of ^{12}C to ^{13}C that is fixed during photosynthesis. The enzyme Rubisco discriminates against ^{13}C relative to ^{12}C during photosynthesis. When stomata are partially closed, faster fixation of ^{12}C leads to an increase in the amount of ^{13}C relative to ^{12}C inside the leaf, and therefore, decreased discrimination against ^{13}C (Francey and Farquhar, 1982; McCarroll and Loader, 2004). Thus, an increase in $\delta^{13}C$ can indicate a rise in relative plant water stress with all else being equal (Farquhar et al., 1989; McNulty and Swank, 1995).

Variation in latewood $\delta^{13}C$ in Douglas-fir trees in the northwest U.S. has been related to air temperature and relative humidity (Barnard et al., 2012) as well as the amount of transpiration during the growing season (Livingston and Spittlehouse, 1996). Atmospheric variables often co-vary, and their relative impacts on tree physiological water stress, including any delayed effects, are not well understood (Fang et al., 2021). In addition, the use of temperature as a primary predictor of tree growth and water stress can be problematic because higher temperatures can impose stress on trees in two distinct ways. First, high temperatures can limit the rate of carbon assimilation in foliage via direct temperature effects on the biochemical reactions involved in photosynthesis (Cai et al., 2008). Second, higher temperatures often indicate higher VPD, which can cause higher rates of transpiration due to open stomata. In response, trees may partially close their stomata at high VPD to avoid hydraulic failure associated with increased tension in the xylem (Fu et al., 2019), which simultaneously decreases the rate of diffusion of carbon dioxide into the foliage. Thus, when using air temperature data alone, it is not possible to tell whether growth at high temperatures is limited by direct temperature effects or VPD-related effects.

The goal of our study was to explore how the intra- and inter-annual variability in daytime and nighttime VPD and total rainfall affect the latewood growth and stable carbon isotope composition of 50-year-old Douglas-fir growing on the west slopes of the Cascade Mountains of Oregon, USA. We focused on latewood because it is formed during the driest and warmest portion of the year when the potential for tree hydraulic stress is greatest. Disentangling the effects of VPD from rainfall is difficult because they tend to be correlated at seasonal timescales (Novick et al., 2016). Thus, we used a moving window analysis to independently test all possible periods of the year when VPD and rainfall were most strongly related to annual latewood growth and carbon isotope composition. Additionally, we evaluated the relative strength of these relationships. Lastly, we explored whether differences in soil water deficits along a steep hillslope gradient altered the effect of VPD and rainfall on latewood growth and $\delta^{13}C$.

We asked:

(a) Over which period of the year are radial growth and $\delta^{13}C$ most highly correlated to VPD and rainfall?
(b) What is the relative sensitivity of radial growth and $\delta^{13}C$ to interannual variability in VPD versus rainfall?
(c) Do differences in soil moisture deficits along a steep hillslope gradient alter the effect of VPD and rainfall on radial growth and $\delta^{13}C$?

2. Materials and methods

2.1. Study site

Our study took place on two north-facing hillslope transects in Watershed 1 (Fig. 1), a 96 ha catchment in the H. J. Andrews Experimental Forest on the west slopes of the Cascade Mountains in central Oregon (44°12′18.8″ N, 122°15′16.2″ W). The transects were at an elevation of ~ 560 m. The climate in the region is characterized by cool, wet winters and warm, dry summers. Mean total annual precipitation over 30 water years (1990–2019) was 2,210 ± 435 mm (Daly et al., 2019) with more than 90 % of annual rainfall occurring from October through June. Precipitation at our study site is dominated by rainfall with transient snowpack during winter months. Mean total annual rainfall during the dry season (July through September) in the 1990–2019 water years was 75 ± 39 mm (Daly et al., 2019).

Watershed 1 is characterized by steep (mean slope = 31°), highly dissected ridges and valleys. Mineral soils are gravelly, silty clay loam. Average depth to bedrock in our study area was 2.3 m and the standard deviation was 1.2 m (Jarecke et al., 2021). Soils are underlain predominantly by altered pyroclastic flows of the Little Butte Formation (Swanson and James, 1975).

The watershed was clearcut from 1962 to 1966 and burned in 1966. There were multiple efforts to re-establish vegetation from 1967 to 1971 including aerial seeding and planting 2- and 3-year-old seedlings (Halpern, 1988). At the time of our study, in 2019, the stand was composed predominantly of second growth Douglas-fir trees (*Pseudotsuga menziesii*, ~40–50 years old), with some bigleaf maple (*Acer macrophyllum*) and Western hemlock (*Tsuga heterophylla*) present. We assessed the height of trees in our study area with LiDAR data (Spies, 2016). The average height of trees was 24 m, and the maximum height was 34 m.

2.2. Climate variables and field data collection

We used meteorological data recorded at the Primary Meteorological Station (PRIMET) at the H. J. Andrews Experimental Forest. The station was located in a small clearing less than a kilometer from our study site. Air temperature and relative humidity (HMP45C probe with Vaisala capacitive relative humidity sensor and a Fenwal Electronics UUT51J1 thermistor, Campbell Scientific) were measured at 1.5 and 4.5 m aboveground. Rainfall (TE525 tipping bucket rain gauge, Texas Electronics) was measured at 1 m above the ground. We used 15 min rainfall, air temperature, and relative humidity data from 1989 to 2019 (Daly et al., 2019), and calculated the VPD from relative humidity and temperature. We aggregated 15 min data to hourly averages and then estimated total daily rainfall and mean daytime and nighttime VPD, where daytime was defined as the intervals of time when solar radiation (Kipp and Zonnen pyranometer with thermopile type sensor, model CM-6B) was greater than 10 W m^{-2} and nighttime defined as intervals of time when solar radiation was less than 10 W m^{-2}. Missing hourly data for air temperature and relative humidity occurred on ~ 3 % of dates between 1989 and 2019. When an observation was missing for a particular day, we used the long-term average daytime air temperature and relative humidity for that day.

Annual latewood growth was estimated from tree cores extracted at 1.3 m above the ground level. We cored 3 dominant trees at each of 9 sites in November 2019. Dominant trees can be more sensitive to climate variation compared to co-dominant and intermediate canopy position

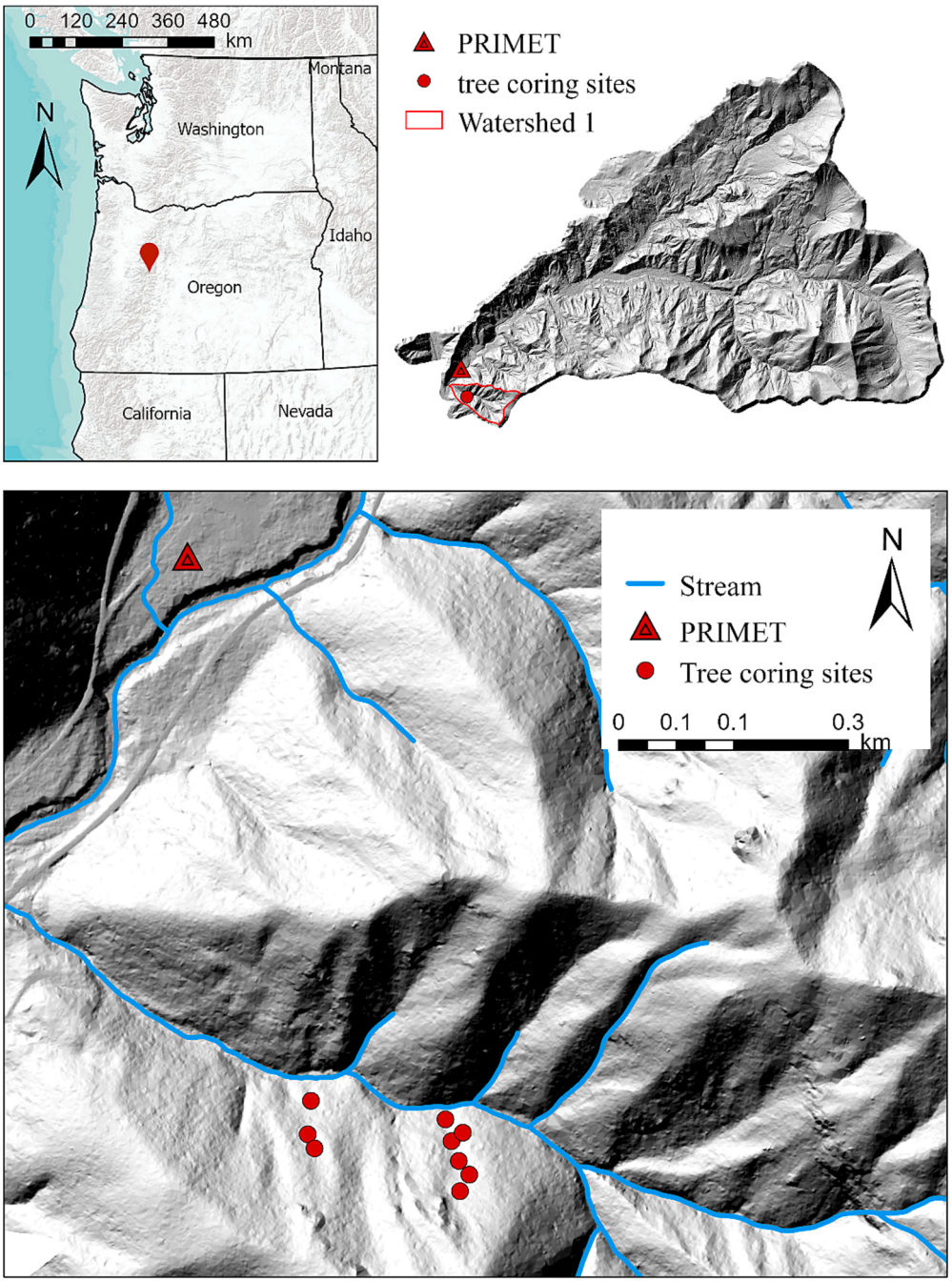

Fig. 1. Location of Watershed 1 at the HJ Andrews Experimental Forest near Blue River, Oregon. Tree cores were collected along two hillslopes at nine sites (red dots). Meteorological data were collected at PRIMET station (red triangle) approximately 1 km from tree coring sites.

trees (Barnard et al., 2012). Thus, the heights of trees at each site were visually inspected, and dominant trees were identified by crowns extending above the average crown height. Additionally, we measured and recorded the diameter of the tree at 1.3 m above the ground level. The mean diameter among all trees ($n = 27$) was 37.5 ± 4.7 cm.

Sites were located approximately 20–40 m apart along two hillslope transects (Fig. 1). Soil moisture sensors (5TM, METER Environment) were installed horizontally into undisturbed soil at each site in October 2018 to record hourly measurements at 50 and 100 cm. The 3 dominant sample trees at each site were located within 10 m of the sensors. The soil moisture deficit at 50 and 100 cm at each site was determined from daily soil water content from March 1 to September 30, 2019 (Fig. 2). Soil water deficit during the growing season was defined as field capacity minus the minimum soil water content. Missing data occurred at 50 cm on several dates during March and April due to insufficient power to the data loggers. Thus, we chose to use the soil water content on April 20, 2019 (Fig. 2) as our estimate for field capacity because it represents the start of soil moisture decline following 368 mm of rainfall between April 1 and 20, 2019. The minimum soil water content was observed at the end of the dry season and before the first major rain event in early September.

2.3. Lab processing of tree cores

We dried, mounted, and sanded tree cores for which latewood and earlywood boundaries for each year's growth were easily observable. All cores were dated, and cross-dating accuracy was checked using COFECHA software (Holmes, 1983). We measured the width of earlywood

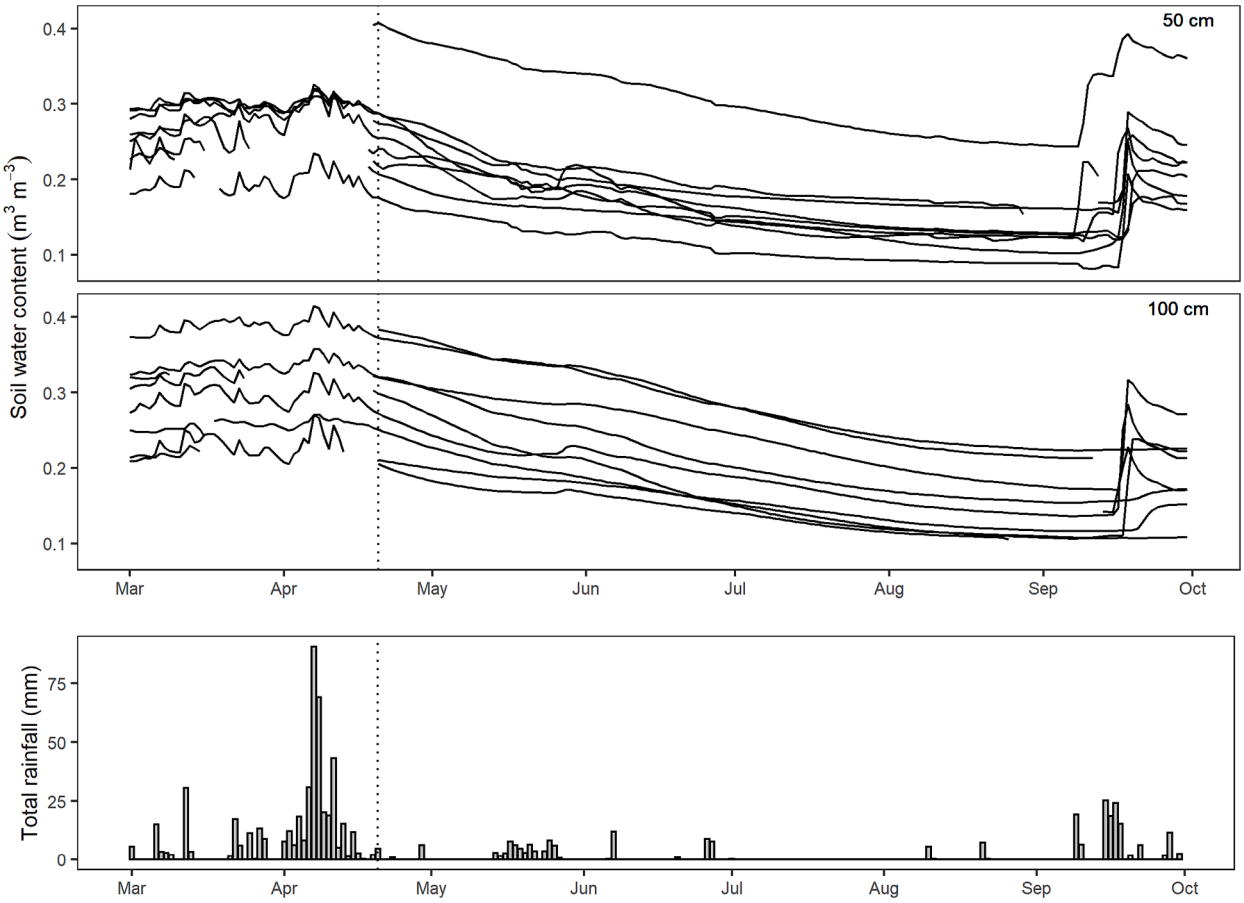

Fig. 2. Soil water content (m^3 m^{-3}) was measured at each of the nine tree coring sites from March 1 to September 30, 2019. Field capacity was estimated as soil water content on April 20, 2019 (dotted line). The soil moisture deficit was defined as the field capacity minus the minimum soil water content observed during the dry season.

and latewood rings along each core with a sliding stage incremental micrometer (Velmex, Inc., Bloomfield, NY, USA, 0.001 mm precision) and Measure J2X software (VoorTech Consulting, Holderness, NH, USA).

Latewood was distinguished from earlywood by a step-change in color. Douglas-fir latewood has narrower and thicker-walled conduits and, as a result, appears darker than earlywood. The transition from large-diameter, thin-walled earlywood tracheids to narrow-diameter, thick-walled latewood tracheids occurs during the summer, resulting in a change in wood density. We calculated the annual latewood basal area increment (BAI), defined as the cross-sectional area of annual latewood growth in each tree, assuming a circular cross section of the stem.

2.4. Isotope analyses

We processed latewood for stable carbon isotope analysis for a subset of years, 1999–2019. We used a rotary Dremel with a 60-grit sanding band to grind the latewood rings into wood powder for each year's growth. We pooled the wood powder from 3 replicate cores per tree for a total of 567 samples (27 trees × 21 years). We identified the beginning of latewood growth within each annual ring by observing a distinct change in color and texture at the boundary between earlywood and latewood. The ground latewood was stored in scintillation vials and subsequently transferred to polyester filter bags (mesh size 25 μm, ANKOM technology, Macedon, NY) which were heat-sealed. We placed the filter bags in glass beakers with an acetic acid-acidified sodium chlorite solution to extract lignin following methods in Rinne et al. (2005), which were modified after Leavitt and Danzer (1993). The reaction was monitored for ~ 5 days and the filter bags were removed from the solution when there was no longer a color change in the solution from bright yellow to clear and sample material appeared white. The filter bags were rinsed several times with deionized water and dried in an oven at 70 °C overnight.

Subsamples of holocellulose weighing between 0.8 and 0.9 mg were prepared for carbon isotope analyses at the Stable Isotope Laboratory at Oregon State University. The samples were subjected to flash combustion using a Carlo Erba NA 1500 elemental analyzer connected in continuous-flow mode to a DeltaPlus isotope ratio mass spectrometer. Daily calibration was performed using the international standard USGS40 (glutamic acid) and the internal lab standard SIL Sucrose. The international standard IAEA-600 (caffeine) was also used as a check standard. The accuracy calculated from 52 check standards was 0.06 ± 0.07 ‰. The $\delta^{13}C$ values were calculated relative to the standard using the equation

$$\delta^{13}C = \left(\frac{R_{sample}}{R_{standard}} - 1\right) 1000,$$

where R represents the ratio of ^{13}C to ^{12}C atoms of the sample or standard. The standard deviation of 51 replicated samples was ± 0.06 ‰.

2.5. Moving window analysis

We used a moving window analysis to determine the period of the year when rainfall and VPD were most strongly related to latewood growth and carbon isotope ratios. There was considerable variation in both average daytime and nighttime VPD (Fig. 3a) as well as total

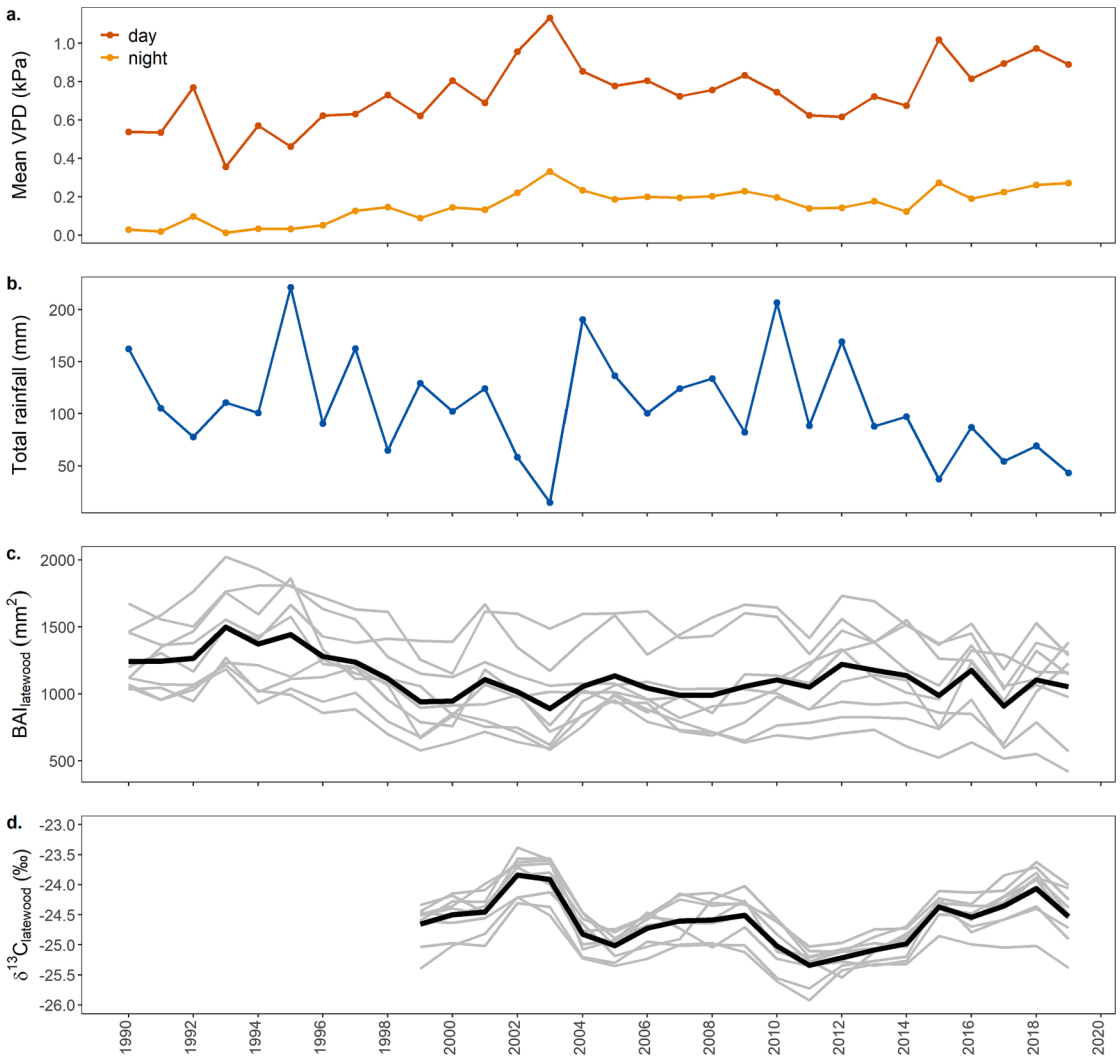

Fig. 3. The average daytime vapor pressure deficit (VPD) and nighttime VPD (a) and total rainfall (b) between June and August from 1990 to 2019. The average latewood basal area increment (BAI) at each site (grey, $n = 9$) and the overall mean BAI among sites (black) over 30 years, 1990–2019 (c). The average latewood $\delta^{13}C$ at each site (grey, $n = 9$) and the overall mean $\delta^{13}C$ (black) over 21 years, 1999–2019 (d). The overall mean values for BAI and $\delta^{13}C$ were used for the moving window analysis.

rainfall (Fig. 3b) during the summer months from 1990 to 2019. We used the average latewood BAI spanning the years 1990–2019 (Fig. 3c) and average latewood $\delta^{13}C$ from 1999 to 2019 (Fig. 3d) as the response variables in the moving window analysis. These variables were examined in relation to the explanatory variables, which included total rainfall, average nighttime VPD, and average daytime VPD.

We performed our analysis using the '*climwin*' package in R (Bailey and van de Pol, 2016). In *climwin*, we used daily climate data to identify the most likely climate predictors of latewood BAI and $\delta^{13}C$, and the period of the year when these climate factors were most relevant. We calculated an average daytime and nighttime VPD and total rainfall for multiple periods between June 1st of the year preceding growth and September 30th of the current year's latewood growth. We used this approach to examine a total of 118,341 time periods or 'windows,' ranging from a minimum duration of 2 days to a maximum duration of 16 months, during which we aggregated each climate variable. By defining our windows over a 16-month period, we were able to capture potential lagged effects of climate on latewood formation and carbon isotopic composition. For each window within the 16-month period ($n = 118,341$), we constructed linear models to examine the relationships between the following variables: daytime VPD and BAI, nighttime VPD and BAI, rainfall and BAI, daytime VPD and $\delta^{13}C$, nighttime VPD and $\delta^{13}C$, and rainfall and $\delta^{13}C$.

To compare the models for each relationship, we used the Akaike information criterion corrected for small sample sizes (AIC_c). The ΔAIC_c for each model is the difference between the model AIC_c and the AIC_c of the null model. The null model for BAI was a horizontal line with the intercept equal to the latewood BAI averaged from 1990 to 2019. The null model for $\delta^{13}C$ was a horizontal line with the intercept equal to the latewood $\delta^{13}C$ averaged from 1999 to 2019. The ΔAIC_c values were used to assess the level of support for each model, indicating whether meteorological conditions during a specific period of the year could explain the variations in latewood growth and carbon isotope composition. The model with the highest improvement over the null model was identified as the most favorable model.

The *climwin* package was also used to estimate model weights, which are posterior model probabilities indicating the likelihood of each model being the best-supported one. The models were ranked based on their weight, from largest to smallest, and the largest model weights were summed until reaching a cumulative value of 0.95. The models included in this sum formed the 95 % model confidence set, which was used to assess the uncertainty in selecting the single best model. A relatively large number of models in the 95 % model confidence set indicated a higher level of uncertainty in choosing the best model. Additionally, we

analyzed the range of climate windows, specifically the opening and closing dates, within the 95 % model confidence set. A small variation in opening and closing dates of the windows in the 95 % confidence set indicated that the linear models in that set were limited to a particular period of the year.

Several climate windows may be equally likely to result in a model with similar ΔAIC_c values due to the exploratory nature of the moving window analysis and fine temporal resolution of the climate data (daily). To assess the likelihood of our best model being chosen by random chance, we repeated the moving window analysis after randomly shuffling the dates in the original dataset to eliminate any true climate signal. This randomization test was repeated 100 times to generate a distribution of ΔAIC_c values. We used the randomization distribution of ΔAIC_c values to estimate the probability of obtaining the observed or smaller values of ΔAIC_c from our single best model. If this probability was less than 0.05, we concluded that our results were unlikely to have occurred purely by random chance. This method of model selection presented several advantages over the traditional reliance on Pearson correlation with monthly or biweekly climate variables. By eliminating dependence on arbitrarily defined time intervals, the moving window analysis reduced the likelihood of type I and II errors while enhancing explanatory power. A more comprehensive discussion of the benefits of the moving window analysis is available in van de Pol et al. (2016) and Rubio-Cuadrado et al. (2022).

2.6. Mixed effects model

We used a linear mixed effect model (R package 'lmer'; Pinheiro et al., 2022) to assess the differences in the effects of daytime VPD and rainfall on the yearly latewood BAI and $\delta^{13}C$ among the nine sampling sites. The average daytime VPD and total rainfall derived from the moving window analysis served as fixed effects, interacting with the site—a categorical variable. We incorporated a random effect for individual sample trees within each site to account for within-site variability. The model residuals were examined to ensure adherence to the assumptions of independence, normality, and constant variance. Furthermore, we tested for temporal autocorrelation among the residuals. To address this autocorrelation, we relaxed the assumption of constant variance for the 'site' factor and incorporated an autoregressive lag 1 correlation structure. Residuals were rechecked to confirm that the modified model structure resulted in homogeneity of the residuals.

We estimated the variance components of the model using restricted maximum likelihood and calculated a pseudo-R^2 to assess how well the interaction terms (VPD × site and rainfall × site) explained the variation in latewood growth and carbon isotope composition. We used the R package 'emmeans' (Lenth, 2023) to estimate and compare the marginal means and confidence intervals of the linear slopes associated with each site. The slope estimates obtained from the linear mixed effects model predicted the effect of VPD and rainfall on yearly latewood BAI and $\delta^{13}C$ at each site ($n = 9$), accounting for the influence of other variables in the model. We examined the relationship between the slope estimates and the growing season soil moisture deficit at depths of 50 and 100 cm to investigate whether local soil moisture availability influenced the impact of climate on latewood growth and carbon isotope composition.

3. Results

3.1. Variability in summer climate, latewood growth, and latewood $\delta^{13}C$

The mean daytime VPD during the summer (June–August) ranged from 0.36 to 1.13 kPa between 1990 and 2019 (Fig. 3a). In contrast, the mean nighttime VPD ranged from 0.01 to 0.33 kPa (Fig. 3a). The total summer rainfall ranged from 14.9 to 221.3 mm (Fig. 3b). The annual radial growth of latewood, measured by the latewood basal area increment (BAI), exhibited substantial variability among the nine sites (Fig. 3c). The average annual latewood BAI between 1990 and 2019 was 1,126 mm^2, with a standard deviation of 469 mm^2. The change in latewood BAI from year to year, both in terms of magnitude and direction, did not demonstrate a consistent trend across the sites. However, when considering the overall mean latewood BAI, there was a notable decrease in the annual latewood growth between 1995 and 2000.

In contrast, the trend in $\delta^{13}C$ was relatively similar among the sites from 1999 to 2019 (Fig. 3d). The average value for $\delta^{13}C$ between 1999 and 2019 was −24.6 ‰ with a standard deviation of 0.5 ‰. The average latewood $\delta^{13}C$ and average latewood BAI were weakly correlated ($R^2 = 0.30$) between 1999 and 2019. The temporal trend in latewood $\delta^{13}C$ generally mirrored that of BAI during extreme dry or wet summers. For example, the driest summers with low rainfall and high VPD, such as 2002 and 2003, corresponded to high $\delta^{13}C$ values and low BAI. Conversely, wet summers, like 2004 and 2005, were associated with relatively low $\delta^{13}C$ values and high BAI.

3.2. Relationships between response variables and climate variables

The optimal climate window, as determined by the best model (with the lowest ΔAIC_c value) showcasing the relationship between each response variable and each climate variable, occurred between May and September (Table 1). This time frame aligns with the latewood formation period of the current year. Other candidate models, falling within the 95 % confidence set, included models with window opening and/or closing dates prior to May (Fig. 4). Less than 10 % of all models were included in the 95 % confidence set for the relationship between BAI and average daytime VPD, $\delta^{13}C$ and average daytime VPD, and $\delta^{13}C$ and total rainfall (Table 1). However, we observed a greater number of models in the 95 % model confidence set for BAI vs. average nighttime VPD (21 %), $\delta^{13}C$ vs. average nighttime VPD (43 %), and BAI vs. total rainfall (77 %). Consequently, this greater number of models in the 95 % confidence set resulted in increased variability in window opening and closing dates (Fig. 4).

We observed a strong negative linear relationship between BAI and average daytime VPD from June 13 to July 15 ($R^2 = 0.71$, Fig. 5a). Similarly, a strong negative relationship was identified between BAI and average nighttime VPD from June 19 to July 14 ($R^2 = 0.66$, Fig. 5b). In contrast, we observed a positive, albeit slightly weaker, relationship between BAI and total rainfall within a narrower window from June 13 to 23 ($R^2 = 0.43$, Fig. 5c). The ΔAIC_c values for the single best models in the cases of BAI vs. daytime VPD and BAI vs. nighttime VPD were significantly lower than the distribution of ΔAIC_c values generated with the randomized data sets ($p < 0.001$, Fig. 5a, 5b). However, the ΔAIC_c value for the best model in the case of BAI vs. total rainfall overlapped with the distribution of ΔAIC_c values generated by the randomization test ($p = 0.02$, Fig. 5c), indicating more uncertainty in the model selection.

We observed a strong positive relationship between $\delta^{13}C$ and average daytime VPD from May 15 to September 28 ($R^2 = 0.80$, Fig. 6a). Additionally, we found a positive, but slightly weaker, relationship between $\delta^{13}C$ and average nighttime VPD within a narrower window from May 17 to June 13 ($R^2 = 0.45$, Fig. 6b). In contrast, a strong negative linear relationship was identified between $\delta^{13}C$ and total rainfall from May 16 to August 14 ($R^2 = 0.69$, Fig. 6c). The ΔAIC_c for the single best model for $\delta^{13}C$ vs. daytime VPD was significantly lower than the distribution of ΔAIC_c values generated by the randomized data sets ($p < 0.001$, Fig. 6a). However, the ΔAIC_c for the single best model for $\delta^{13}C$ vs. nighttime VPD was not statistically different from the distribution of ΔAIC_c values generated by the randomized data ($p = 0.34$, Fig. 6b). We also found that the ΔAIC_c value for the single best model in the case of $\delta^{13}C$ vs. total rainfall overlapped the tail end of the distribution of ΔAIC_c values generated by the randomized data ($p = 0.02$, Fig. 6c).

Table 1
Summary of results from the moving window analysis to identify the relationship between latewood BAI and $\delta^{13}C$ and each of the climate variables—daytime vapor pressure deficit (VPD), nighttime VPD, and rainfall. Mean daytime and nighttime VPD and total rainfall were estimated over all possible window opening and closing dates from September 30 of each growth year to June 1 of the previous year. Linear models between explanatory and response variables were evaluated with Akaike information criterion (AICc).

Explanatory variable	Response variable	Sample Size (years)	Climate Window of "Best" Model	ΔAICc	Linear model		Percent of models in 95 % confidence set	*p* of the randomization test
					R^2	*p*		
Average daytime VPD (kPa)	$\delta^{13}C$	21	May 15 – September 28	−30.82	0.80	<0.001	4	<0.001
	BAI	30	June 13 – July 15	−35.03	0.71	<0.001	7	<0.001
Average nighttime VPD (kPa)	$\delta^{13}C$	21	May 17 – June 13	−9.68	0.45	<0.001	43	0.34
	BAI	30	June 19 – July 14	−29.90	0.66	<0.001	21	<0.001
Total rainfall (mm)	$\delta^{13}C$	21	May 16 – August 14	−21.56	0.69	<0.001	3	0.02
	BAI	30	June 13 – June 23	−14.62	0.43	<0.001	77	0.19

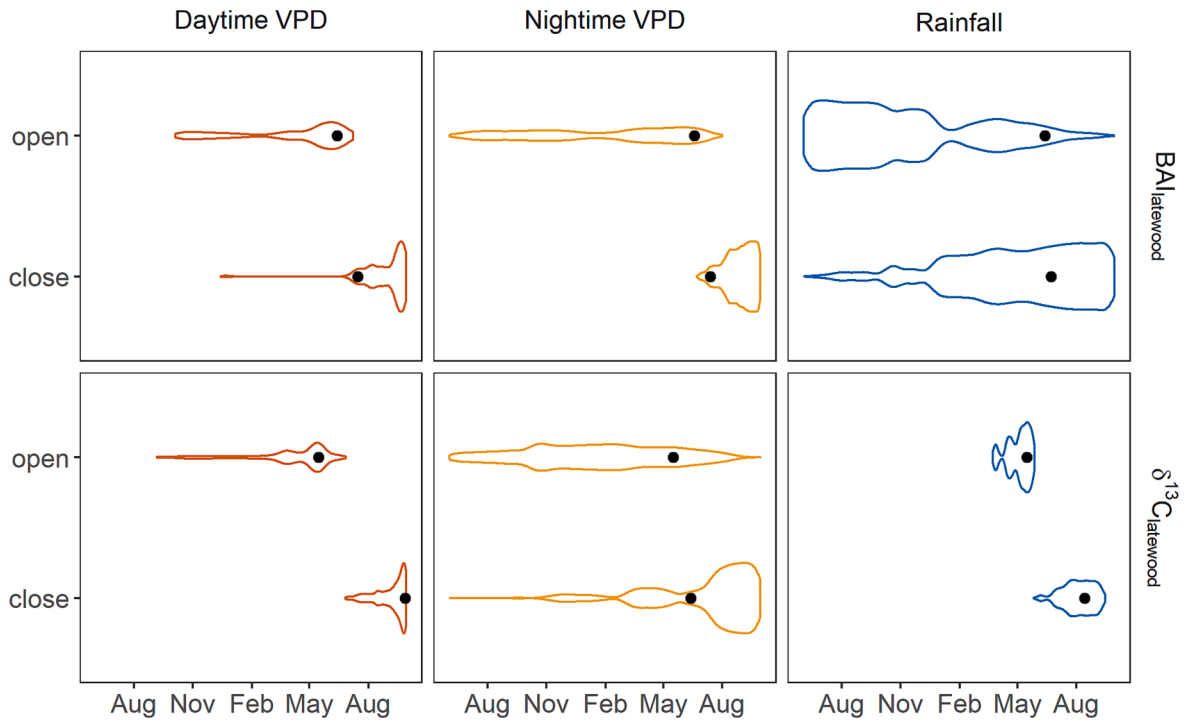

Fig. 4. Distribution of window opening and closing dates that make up the top 95 % of model weights (the 95 % model confidence set) after a moving window analysis of all possible time windows (n = 118,341). The black dots represent the window opening and closing dates for the model with the lowest ΔAICc that describes the "best" linear relationship between each response variable, BAI and $\delta^{13}C$, and each climate variable, average daytime vapor pressure deficit (VPD), average nighttime VPD, and total rainfall.

3.3. The influence of VPD and rainfall on latewood growth and $\delta^{13}C$ across sites

The fixed effects in our model, namely the mean daytime VPD × site and total rainfall × site, accounted for approximately 35 % of the variation in latewood BAI and 41 % of the variation in latewood $\delta^{13}C$. However, the overall interactive effect of daytime VPD × site in the mixed effect model for BAI was not statistically significant (F = 0.38, p = 0.93) nor was the effect of rainfall × site (F = 0.42, p = 0.91). Similarly, we found no evidence of a significant interactive effect of VPD × site (F = 1.18, p = 0.31) or rainfall × site (F = 0.56, p = 0.81) in the mixed effect model for $\delta^{13}C$. Although the interaction terms were not significant in our mixed effects models for BAI and $\delta^{13}C$, we estimated the marginal slopes to examine potential practical differences in the effects of VPD and rainfall among sites.

The marginal slopes of the linear trends of BAI vs. VPD were statistically different from zero for all sites except two ($p < 0.05$, Fig. 7a). In the best model for predicting mean BAI, the average daytime VPD, estimated between June 13 to July 15, ranged from 0.50 to 1.19 kPa over a span of 30 years, representing a difference of 0.69 kPa. Marginal slope estimates from our mixed effects model indicated a decrease in latewood BAI by 289 to 600 mm^2 for every 1 kPa increase in VPD (95 % CI = -932 to + 26 mm^2). The slope estimates for the change in BAI with a 1 kPa increase in VPD did not show strong correlation with the soil moisture deficit at 50 cm (*data not shown*), but they exhibited a weak negative trend with the soil moisture deficit at 100 cm (Fig. 7a). Conversely, the marginal slopes of BAI vs. total rainfall were not statistically different from zero at any of the sites (p = 0.26–0.99, Fig. 7b). The range in total rainfall within the climate window for the best model (June 13 to June 23) spanned from 0 to 66 mm. The predicted change in latewood growth for a 100 mm increase in rainfall varied from −112 to + 238 mm^2 among sites (95 % CI = -415 to + 653 mm^2).

The marginal slopes of $\delta^{13}C$ vs. VPD were statistically significant for all sites ($p < 0.02$, Fig. 8a). However, we did not observe any meaningful correlation between the slope estimates and the soil moisture deficit at 50 or 100 cm. The average daytime VPD within the window of the best model for $\delta^{13}C$ (May 15 to September 28) ranged from 0.73 to 1.16 kPa, representing a difference of 0.43 kPa. The model predicted an increase in latewood $\delta^{13}C$ by 1.6 to 3.4 ‰ with a 1 kPa increase in VPD (95 % CI = 0.3 to 4.7 ‰). In contrast, the marginal slopes of $\delta^{13}C$ vs. total rainfall

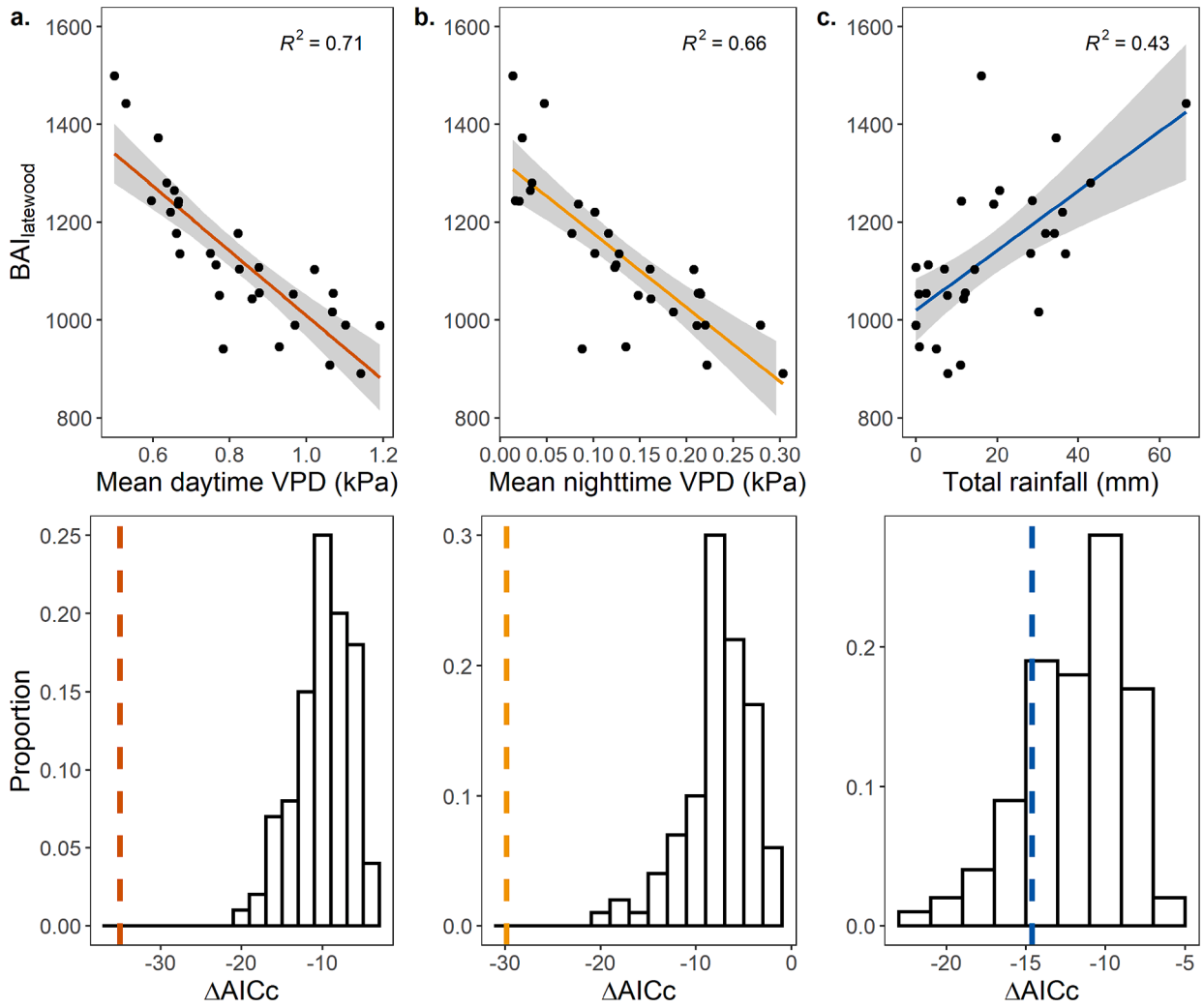

Fig. 5. The relationship between mean latewood basal area increment (BAI) and average daytime vapor pressure deficit (VPD, a), average nighttime VPD (b), and total rainfall (c) for the best model based on the moving window analysis. We tested whether the ΔAIC_c value for the best model (dashed line) differed from the distribution of ΔAIC_c values from the moving window analysis that removed any true climate signal by randomly rearranging the date in the original dataset.

were not statistically different from zero at any of the sites (p = 0.16–0.95, Fig. 8b). The range in total rainfall within the climate window for the best model (May 16 to August 14) was 37 to 298 mm, a difference of 261 mm. The predicted change in latewood $\delta^{13}C$ for a 100 mm increase in rainfall ranged from −0.1 to + 0.1 ‰ among sites (95 % CI = -0.3 to + 0.3 ‰).

4. Discussion

Our study tested how vapor pressure deficit (VPD) and rainfall influenced latewood growth and physiological water stress in Douglas-fir trees growing in a Mediterranean climate. We found that latewood growth was strongly affected by daytime VPD during the period from mid-June to mid-July while the amount and timing of rainfall was less influential. In contrast, both daytime VPD and the amount of rainfall between May and September were strongly related to latewood $\delta^{13}C$, indicating that the degree of physiological water stress is determined by climatic conditions over a longer period of the growing season. We also found considerable variation in latewood growth and $\delta^{13}C$ among sites. However, the relationships between climate variables, latewood growth, and carbon isotope composition appeared to be relatively unaffected by the local soil water deficit on the north-facing slope in our study.

4.1. Summer vapor pressure deficits influenced latewood growth and carbon isotope composition

Increasing average daytime and nighttime VPD from mid-June to mid-July led to a decrease in yearly latewood growth. This result is consistent with previous studies that found increased temperature and VPD can induce a decrease in growth of Douglas-fir on the west slope of the Cascade Mountains (Beedlow et al., 2013; Restaino et al., 2016). During the period of our analysis (1990–2019), average daytime VPD from mid-June to mid-July ranged from ~ 0.5 to 1.2 kPa, with average daytime temperature ranging from ~ 16 to 23 °C. We would not expect stomatal conductance or photosynthesis to be constrained under these conditions as the optimal temperature for photosynthesis in Douglas-fir in western Oregon is around 20 °C, with rates declining rapidly above 25 °C (Lewis et al., 2001). However, the average maximum daytime temperature from June 13 to July 15 during 1990–2019 was much warmer, ranging from ~ 29 to 40 °C, with maximum daytime VPD ranging from ~ 2.7 to 6.2 kPa. As a result, the correlation of latewood growth to average daytime and nighttime VPD may have served as a proxy for the number of days when high midday temperature and VPD induced significant tree water deficits. Previous research suggests that most tree growth occurs overnight and in the early morning after trees have recovered their water deficit, and turgor is optimal for cell division and expansion (Zweifel et al., 2021). Thus, it is plausible that the

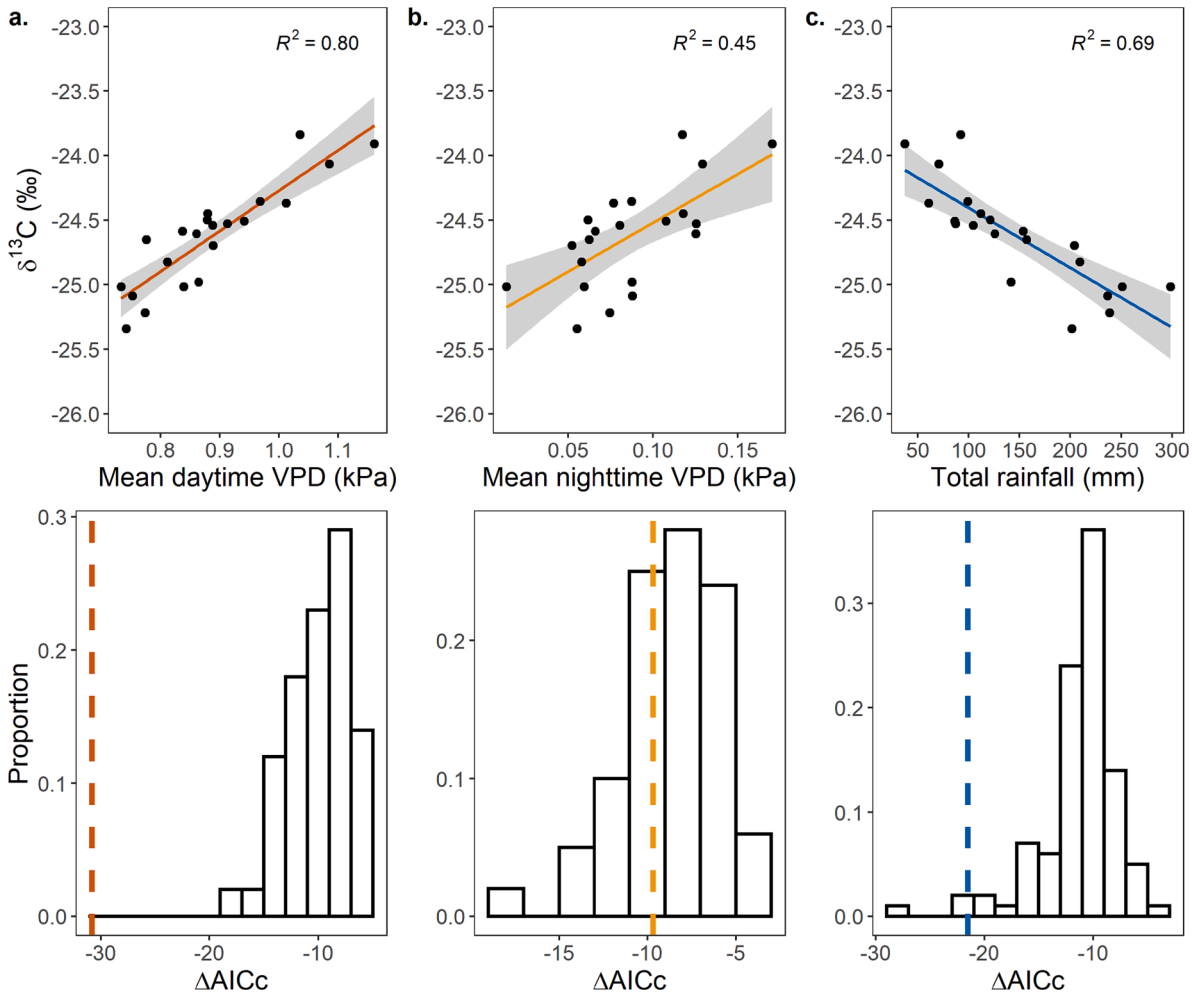

Fig. 6. The relationship between mean latewood $\delta^{13}C$ and average daytime vapor pressure deficit (VPD, a), average nighttime VPD (b), and total rainfall (c) for the best model based on the moving window analysis. We tested whether the ΔAIC_c value for the best model (dashed line) differed from the distribution of ΔAIC_c values from the moving window analysis that removed any true climate signal by randomly rearranging the date in the original dataset.

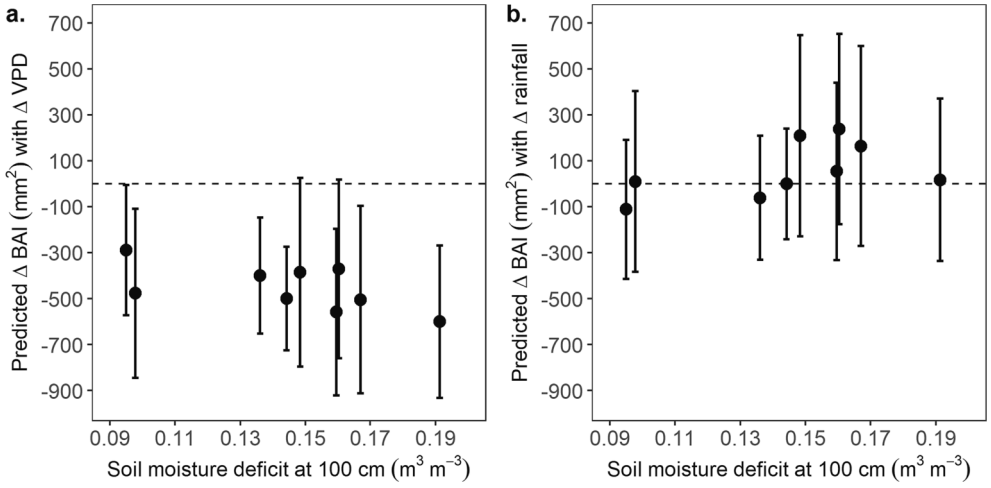

Fig. 7. The marginal slopes for individual sites represent the predicted change in latewood basal area increment (BAI) with an increase in daytime vapor pressure deficit (VPD) by 1 kPa (a) and with an increase in rainfall by 100 mm (b). Error bars represent 95 % confidence intervals. The marginal slopes describing the effect of VPD on BAI were weakly correlated to sites' soil moisture deficit at 100 cm (R^2 = 0.38). Marginal slopes for the effect of rainfall did not differ from zero.

reduction in latewood growth was strongly linked to periods when elevated VPD from mid-June to mid-July led to significant tree water deficits.

Elevated VPD also resulted in increased physiological water stress, as indicated by increased $\delta^{13}C$ values. Latewood $\delta^{13}C$ was positivley correlated with the average daytime VPD between May and September,

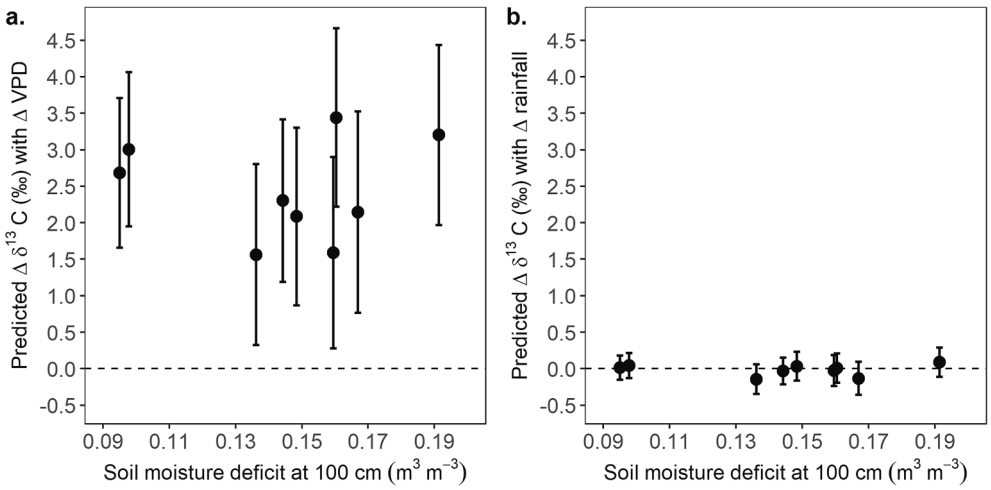

Fig. 8. The marginal slopes for individual sites represent the predicted change in latewood $\delta^{13}C$ for an increase in daytime vapor pressure deficit (VPD) by 1 kPa (a) and for an increase in rainfall by 100 mm (b). Error bars represent 95 % confidence intervals. The marginal slopes describing the effect of VPD and rainfall on $\delta^{13}C$ were not correlated to sites' soil moisture deficit at 100 cm. Marginal slopes for the effect of rainfall did not differ from zero.

as well as with average nighttime VPD between May and June. However, there was more uncertainty in the best model for nighttime VPD versus latewood $\delta^{13}C$ compared to daytime VPD versus $\delta^{13}C$. This was evident by the greater number of models included in the 95 % model confidence set and lack of distinction between the ΔAICc value for the best model and the distribution of ΔAICc values obtained from the randomization tests.

The strong influence of VPD on the latewood $\delta^{13}C$ of Douglas-fir agrees with other studies that have reported elevated values of latewood $\delta^{13}C$ in response to increased temperatures and decreased relative humidity in summer dry, winter wet climates (Barnard et al., 2012; Livingston and Spittlehouse, 1996). Noteably, the climate window for daytime VPD versus $\delta^{13}C$ (May–September) was much wider than the one observed for daytime VPD vs. BAI, which was limited to June and July. This broader window for the influence of VPD on latewood $\delta^{13}C$ could be attributed to transitions between phases of latewood formation. The formation of latewood involves two distinct phases: cell enlargement and cell wall thickening. Cell enlargement, which we measured as latewood growth, has been documented to last approximately 17 days in Douglas-fir in the Cascade Range (Emmingham, 1974). In contrast, cell wall thickening is a longer process and contributes to the majority of cellulose accumulation in latewood biomass (Cuny et al., 2015). Thus, the phase of cell wall thickening, which affect the $\delta^{13}C$ composition, may integrate climatic conditions over a greater portion of the growing season (Belmecheri et al., 2018). This could explain the broader climate window found for the best model that describes the relationship between latewood $\delta^{13}C$ and VPD.

4.2. Rainfall totals influenced the latewood carbon isotope composition but not latewood growth

Douglas-fir trees can also experience significant water deficits due to limited soil moisture, making them sensitive to both rainfall and temperature (Little et al., 1995; Zhang et al., 1999; Lo et al., 2010). However, because Douglas-fir trees grow across a wide range of regional climates and elevations, studies have reported mixed results concerning the timing and directionality of climate-growth relationships (Bower et al., 2005; Chen et al., 2010; Griesbauer and Green, 2010; Lo et al., 2010). For example, Barnard et al. (2012) examined annual growth of Douglas-fir and found no correlation between annual growth and rainfall, temperature, or relative humidity. Similarly, Livingston and Spittlehouse (1996) did not find a relationship between latewood growth and soil water deficit. Conversely, Robertson et al. (1990) showed that latewood growth of Douglas-fir increased with increasing spring rainfall and decreased with rising summer temperatures. These varying outcomes highlight the complexity of climate-growth relationships in Douglas-fir growing across a diversity of local and regional conditions.

We were unable to examine long-term soil water deficits in our study. The use of long-term soil moisture data, if available for our study area, would have allowed us to directly test the impact of soil moisture deficits on radial growth and $\delta^{13}C$. However, we did not find a specific time of year in which latewood BAI was sensitive to interannual variability in rainfall totals. Although we observed a positive correlation between latewood growth and rainfall, the ΔAIC_c of the best model overlapped the ΔAIC_c values generated from the randomizaiton test. This indicated that the best model for rainfall vs. BAI was just as likely to be selected by random chance. Furthermore, the 95 % confidence set for rainfall vs. BAI comprised a relatively large number of models (77 %), providing additional evidence that latewood growth was not strongly influenced by a specific period of rainfall accumulation. The considerable uncertainty in the rainfall signal in our study implies that rainfall might not have captured the interannual variability in plant-available water. Interestingly, only 6 % of models in the 95 % confidence set for rainfall as a predictor of growth had window opening and closing dates during the summer of the current year's growth. However, among the models with summer windows, we found that 70 % indicated a positive relationship between rainfall and latewood growth. This suggests that despite the lack of evidence that a particular window of time was consequential, increased rainfall amounts during the summer had a positive impact on growth. The positive effect of rainfall on latewood BAI was likely due to rainfall reducing VPD given that relatively small amounts of rainfall during the summer months are not likely to have a large effect on soil moisture. The stronger influence of VPD relative to rainfall aligns with previous research that suggests that heat-driven increases in VPD during the summer can significantly reduce primary production in Douglas-fir, regardless of rainfall amounts (Fu et al., 2022; Jarecke et al., 2023; Jiang et al., 2019; Novick et al., 2016).

In contrast with the latewood growth results, we found that total rainfall from May to August was a strong predictor of latewood $\delta^{13}C$, with $\delta^{13}C$ decreasing with increased rainfall. The ΔAIC_c value for the best model using total rainfal vs. $\delta^{13}C$ overlapped with the tail of the distribution of ΔAIC_c values from the randomization tests. Despite this overlap, the low percentage of models in the 95 % confidence set (~3%) provided evidence that the rainfall accumulation between May and August was a meaningful predictor of latewood $\delta^{13}C$. While our results indicated that latewood $\delta^{13}C$ is influenced by both rainfall and VPD over the growing season, it's important to note that mean daytime VPD between May and September and total rainfall between May and August

were strongly correlated between 1999 and 2019 (Fig. 9).

Disentangling the two drivers of moisture limitation—reduced rainfall and increased atmospheric VPD—is difficult because they co-vary at coarse timescales in Mediterranean climates. The trees selected for this study were located on steep, north-facing slopes and growing in relatively deep (>2 m) soils (Jarecke et al., 2021). Previous research by Brooks et al. (2002) demonstrated that hydraulic redistribution of water from depths below 60 cm supplied approximately 40 % of the daily transpiration in a Douglas-fir stand during the summer dry season. Consequently, higher amounts of rainfall during the summer would contribute to shallow soil moisture and benefit tree growth. However, the timing of rainfall may not be as critical in areas where trees have deep roots and reliable access to subsurface water. Instead, the timing of rainfall might be more important for growth in systems with relatively limited subsurface water storage capacities, such as shallow soils or shallow rooting zone, which are quickly depleted during the growing season (Hahm et al., 2019).

4.3. Interactive effect of climate variables and local soil water deficits on latewood growth and $\delta^{13}C$

The declines in latewood BAI that we observed with increasing VPD are meaningful considering how a reduction in latewood radial growth affects overall wood density (Martinez-Meier et al., 2008) and efficiency of water transport (Domec and Gartner, 2002). For example, in our study area, a 5 °C increase in average daytime air temperature corresponds to a rise in VPD by 1 kPa. We observed that an increase in VPD by 1 kPa resulted in a reduction in latewood BAI ranging from 289 to 600 mm^2 among our sites. A difference in ~ 300 mm^2 among sites is 50 % of the observed range in mean latewood growth across all sites (~600 mm^2) between 1990 and 2019. Similarly, we saw a meaningful range in the marginal slopes describing the change in $\delta^{13}C$ (1.6 to 3.4 ‰) with an increase in VPD by 1 kPa. The marginal slopes differed from zero for all sites, suggesting that trees across all sites were susceptible to increased physiological water stress with increased daytime VPD. However, the results of our linear mixed effects models suggested that the effect of VPD on latewood BAI and $\delta^{13}C$ did not differ significantly among sites.

It's important to note that our ability to delve deeper into the influence of soil moisture was limited due to the availability of only one year of data. As a result, we were unable to investigate how intra- and inter-annual variation in soil moisture influenced tree growth and water stress. Instead, we explored how site-to-site differences in the soil moisture deficit over a single growing season modified the climate-growth and climate-water stress relationships that were determined from the moving window analysis. Soil water deficit, ranging from 0.09 $m^3\,m^{-3}$ to 0.2 $m^3\,m^{-3}$, did not significantly modify the impact of VPD on latewood BAI or $\delta^{13}C$. This suggested that differences in soil moisture availability did not play a substantial role in mitigating the adverse effects of seasonal aridity in our study area.

5. Conclusions

The Pacific Northwest has experienced unprecedented warming and extreme heat events in the 21st century (Heeter et al., 2023). Increased air temperatures during summer have increased baseline aridity, which is expected to exacerbate the effects of extreme heat and drought events on tree growth and recovery in seasonally dry climates (Huang et al., 2018; Williams et al., 2010). Our study tested how inter- and intra-annual vapor pressure deficit (VPD) and rainfall correlated to latewood growth (measured as latewood BAI) and physiological water stress (measured as latewood $\delta^{13}C$) of 50-year-old Douglas-fir trees. Latewood $\delta^{13}C$ was most strongly correlated to mean daytime VPD and total rainfall over the spring to summer growing season. In contrast, latewood growth was sensitive to daytime VPD in early summer but not to the timing and amounts of rainfall. We conclude that increases in VPD during summer are likely to reduce latewood growth and increase water stress in a Mediterranean climate with a distinct dry season.

The growing season soil moisture availability did not exert a strong control on climate-growth or climate-water stress relationships in our study. However, the role of soil moisture in mitigating tree water stress requires further investigation and will be critical for informing forest management decisions. For example, forest managers in the Pacific Northwest have implemented forest thinning strategies to enhance drought resilience. However, if tree water stress stems primarily from atmospheric aridity, then thinning could prove ineffective for mitigating drought and may even worsen physiological water stress by intensifying atmospheric aridity below the canopy. Additional studies using mechanistic modelling and field manipulation are critical to disentangling the relative effects of VPD and soil moisture on tree water stress to develop a more comprehensive understanding of the factors governing forest

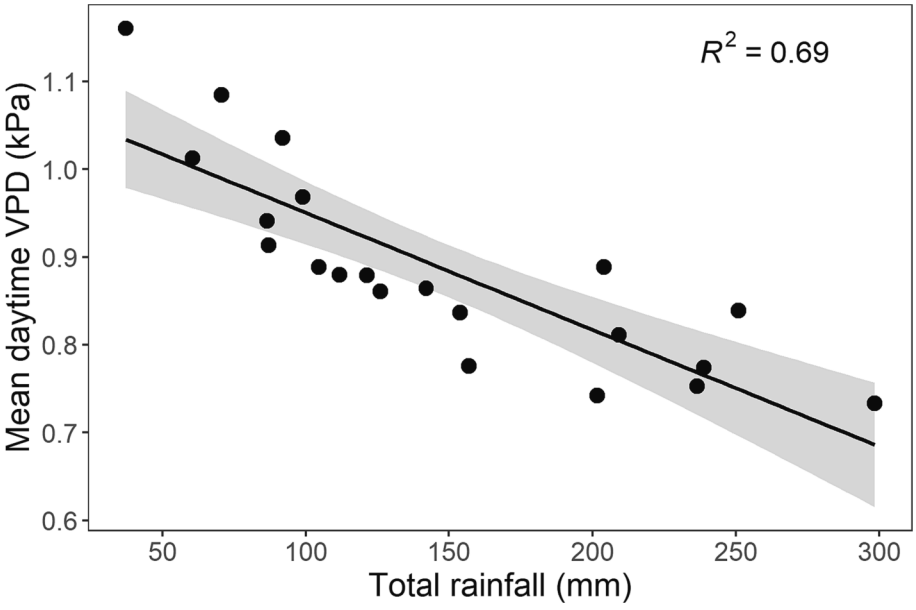

Fig. 9. From 1999 to 2019, there was a strong relationship between the total rainfall from May 16 to August 14 and the mean daytime VPD from May 15 to September 28.

vulnerability to increased aridity.

CRediT authorship contribution statement

Karla M. Jarecke: Conceptualization, Methodology, Software, Formal analysis, Investigation, Data curation, Writing – original draft, Writing – review & editing, Visualization, Project administration. **Kevin D. Bladon:** Conceptualization, Resources, Writing – review & editing, Supervision, Project administration, Funding acquisition. **Frederick C. Meinzer:** Conceptualization, Writing – review & editing. **Steven M. Wondzell:** Conceptualization, Resources, Writing – review & editing, Supervision, Project administration, Funding acquisition.

Declaration of Competing Interest

The authors declare that they have no known competing financial interests or personal relationships that could have appeared to influence the work reported in this paper.

Data availability

Meteorological and tree ring data are publicly available via the Andrews Forest database.

Acknowledgments and Data

We thank the HJ Andrews staff for their support with project logistics and access to facilities. We thank Melissa Mauk, Ellen Luedloff, Jessica Blunn, David Moy, and Haley Weir for their assistance with tree core collection, tree ring dating, and preparation of cellulose for carbon isotope analysis. Andrew Merschel and James Johnston provided guidance with dendrochronology methods and tree ring dating and Jennifer McKay analyzed our samples for stable carbon isotopes at the Stable Isotope Laboratory at Oregon State University. The data used in this study were made available by the HJ Andrews Experimental Forest research program, funded by the National Science Foundation's Long-Term Ecological Research Program (LTER7 DEB 1440409), USDA Forest Service Pacific Northwest Research Station, and Oregon State University. Tree ring widths and carbon isotope ratios are publicly available via the Andrews Forest database (http://andlter.forestry.oregonstate.edu/data/abstract.aspx?dbcode = TV085) in addition to the LiDAR-based DEM (http://andlter.forestry.oregonstate.edu/data/abstract.aspx?dbcode = GI010) and meteorological data (http://andlter.forestry.oregonstate.edu/data/abstract.aspx?dbcode = MS001).

References

Allen, C.D., Breshears, D.D., McDowell, N.G., 2015. On underestimation of global vulnerability to tree mortality and forest die-off from hotter drought in the Anthropocene. Ecosphere 6, 1–55. https://doi.org/10.1890/ES15-00203.1.

Bailey, L.D., van de Pol, M., 2016. climwin: An R Toolbox for Climate Window Analysis. PLoS One 11, e0167980.

Barnard, H.R., Brooks, J.R., Bond, B.J., 2012. Applying the dual-isotope conceptual model to interpret physiological trends under uncontrolled conditions. Tree Physiol. 32, 1183–1198. https://doi.org/10.1093/treephys/tps078.

Beedlow, P.A., Lee, E.H., Tingey, D.T., Waschmann, R.S., Burdick, C.A., 2013. The importance of seasonal temperature and moisture patterns on growth of Douglas-fir in western Oregon, USA. Agric. For. Meteorol. 169, 174–185. https://doi.org/10.1016/j.agrformet.2012.10.010.

Belmecheri, S., Wright, W.E., Szejner, P., Morino, K.A., Monson, R.K., 2018. Carbon and oxygen isotope fractionations in tree rings reveal interactions between cambial phenology and seasonal climate. Plant Cell Environ. 41, 2758–2772. https://doi.org/10.1111/pce.13401.

Bower, A.D., Thomas Adams, W., Birkes, D., Nalle, D., 2005. Response of annual growth ring components to soil moisture deficit in young, plantation-grown Douglas-fir in coastal British Columbia. Can. J. For. Res. 35, 2491–2499. https://doi.org/10.1139/x05-146.

Breshears, D.D., Adams, H.D., Eamus, D., Mcdowell, N.G., Law, D.J., Will, R.E., Williams, A.P., Zou, C.B., 2013. The critical amplifying role of increasing atmospheric moisture demand on tree mortality and associated regional die-off. Front. Plant Sci. 4, 2–5. https://doi.org/10.3389/fpls.2013.00266.

Brooks, J.R., Meinzer, F.C., Coulombe, R., Gregg, J., 2002. Hydraulic redistribution of soil water during summer drought in two contrasting Pacific Northwest coniferous forests. Tree Physiol. 22, 1107–1117. https://doi.org/10.1093/treephys/22.15-16.1107.

Cai, T., Flanagan, L.B., Jassal, R.S., Black, T.A., 2008. Modelling environmental controls on ecosystem photosynthesis and the carbon isotope composition of ecosystem-respired CO_2 in a coastal Douglas-fir forest. Plant Cell Environ. 31, 435–453. https://doi.org/10.1111/j.1365-3040.2008.01773.x.

Case, M.J., Peterson, D.L., 2005. Fine-scale variability in growth climate relationships of Douglas-fir, North Cascade Range, Washington. Can. J. For. Res. 35, 2743–2755. https://doi.org/10.1139/x05-191.

Chen, P.Y., Welsh, C., Hamann, A., 2010. Geographic variation in growth response of Douglas-fir to interannual climate variability and projected climate change. Glob. Chang. Biol. 16, 3374–3385. https://doi.org/10.1111/j.1365-2486.2010.02166.x.

Cuny, H.E., Rathgeber, C.B.K., Frank, D., Fonti, P., Makinen, H., Prislan, P., Rossi, S., Del Castillo, E.M., Campelo, F., Vavrčík, H., Camarero, J.J., Bryukhanova, M.V., Jyske, T., Gricar, J., Gryc, V., De Luis, M., Vieira, J., Cufar, K., Kirdyanov, A.V., Oberhuber, W., Treml, V., Huang, J.G., Li, X., Swidrak, I., Deslauriers, A., Liang, E., Nojd, P., Gruber, A., Nabais, C., Morin, H., Krause, C., King, G., Fournier, M., 2015. Woody biomass production lags stem-girth increase by over one month in coniferous forests. Nat. Plants 1, 1–6. https://doi.org/10.1038/nplants.2015.160.

Daly, C., Schulze, M., McKee, W., 2019. Meteorological data from benchmark stations at the HJ Andrews Experimental Forest, 1957 to present. Long-Term Ecological Research. https://doi.org/10.6073/pasta/c021a2ebf1f91adf0ba3b5e53189c84f.

Domec, J.C., Gartner, B.L., 2002. Age- and position-related changes in hydraulic versus mechanical dysfunction of xylem: inferring the design criteria for Douglas-fir wood structure. Tree Physiol. 22, 91–104. https://doi.org/10.1093/treephys/22.2-3.91.

Emmingham, W.H., 1974. Physiological responses of four Douglas-fir populations in three contrasting field environments. Oregon State University, Corvallis, OR.

Fang, Y., Leung, L.R., Wolfe, B.T., Detto, M., Knox, R.G., McDowell, N.G., Grossiord, C., Xu, C., Christoffersen, B.O., Gentine, P., Koven, C.D., Chambers, J.Q., 2021. Disentangling the effects of vapor pressure deficit and soil water availability on canopy conductance in a seasonal tropical forest during the 2015 El Niño drought. J. Geophys. Res. Atmos. 126, 1–20. https://doi.org/10.1029/2021JD035004.

Farquhar, G.D., Ehleringer, J.R., Hubick, K.T., 1989. Carbon isotope discrimination and photosynthesis. Ann. Rev. Plant Biol. 40, 503–537.

Ficklin, D.L., Novick, K.A., 2017. Historic and projected changes in vapor pressure deficit suggest a continental-scale drying of the United States atmosphere. J. Geophys. Res.-Atmos. 2061–2079 https://doi.org/10.1002/2016JD025855.

Francey, R.J., Farquhar, G.D., 1982. An explanation of C13/C12 variations in tree rings. Nature 297, 28–31.

Fu, Z., Ciais, P., Prentice, I.C., Bastos, A., Luo, X., Green, J.K., Gentine, P., Makowski, D., Stoy, P.C., Yang, H., Hajima, T., 2022. Atmospheric dryness reduces photosynthesis along a large range of soil water deficits. Nat. Commun. 1–10 https://doi.org/10.1038/s41467-022-28652-7.

Fu, X., Meinzer, F.C., Woodruff, D.R., Liu, Y., Smith, D.D., McCulloh, K.A., Howard, A.R., 2019. Coordination and trade-offs between leaf and stem hydraulic traits and stomatal regulation along a spectrum of isohydry to anisohydry. Plant Cell Environ. 42, 2245–2258. https://doi.org/10.1111/pce.13543.

Griesbauer, H.P., Green, D.S., 2010. Assessing the climatic sensitivity of Douglas-fir at its northern range margins in British Columbia, Canada. Trees - Structure and Function 24, 375–389. https://doi.org/10.1007/s00468-009-0407-z.

Grossiord, C., Buckley, T.N., Cernusak, L.A., Novick, K.A., Poulter, B., Siegwolf, R.T.W., Sperry, J.S., McDowell, N.G., 2020. Plant responses to rising vapor pressure deficit. New Phytol. 226, 1550–1566. https://doi.org/10.1111/nph.16485.

Hahm, W.J., Dralle, D.N., Rempe, D.M., Bryk, A.B., Thompson, S.E., Dawson, T.E., Dietrich, W.E., 2019. Low subsurface water storage capacity relative to annual rainfall decouples Mediterranean plant productivity and water use from rainfall variability. Geophys. Res. Lett. 6544–6553 https://doi.org/10.1029/2019GL083294.

Halpern, C.B., 1988. Early successional pathways and the resistance and resilience of forest communities. Ecol. Soc. Am. 69, 1703–1715.

Heeter, K.J., Harley, G.L., Abatzoglou, J.T., Anchukaitis, K.J., Cook, E.R., Coulthard, B.L., Dye, L.A., Homfeld, I.K., 2023. Unprecedented 21st century heat across the Pacific Northwest of North America. npj Clim. Atmos. Sci. 6, 5. https://doi.org/10.1038/s41612-023-00340-3.

Holmes, R.L., 1983. Computer-assisted quality control in tree-ring dating and measurement. Tree-Ring Bull. 43, 11.

Huang, M., Wang, X., Keenan, T.F., Piao, S., 2018. Drought timing influences the legacy of tree growth recovery. Glob. Chang. Biol. 24, 3546–3559. https://doi.org/10.1111/gcb.14294.

Jarecke, K.M., Bladon, K.D., Wondzell, S.M., 2021. The influence of local and nonlocal factors on soil water content in a steep forested catchment. Water Resour. Res. 57, 1–21. https://doi.org/10.1029/2020wr028343.

Jarecke, K.M., Hawkins, L.R., Bladon, K.D., Wondzell, S.M., 2023. Carbon uptake by Douglas-fir is more sensitive to increased temperature and vapor pressure deficit than reduced rainfall in the western Cascade Mountains, Oregon, USA. Agric. For. Meteorol. 329, 109267 https://doi.org/10.1016/j.agrformet.2022.109267.

Jiang, Y., Kim, J.B., Trugman, A.T., Kim, Y., Still, C.J., 2019. Linking tree physiological constraints with predictions of carbon and water fluxes at an old-growth coniferous forest. Ecosphere 10. https://doi.org/10.1002/ecs2.2692.

Leavitt, S.W., Danzer, S.R., 1993. Method for batch processing small wood samples to holocellulose for stable-carbon isotope analysis. Anal. Chem. 65, 87–89. https://doi.org/10.1021/ac00049a017.

Lenth, R., 2023. _emmeans: Estimated Marginal Means, aka Least-Squares Means_. R Package Version 1 (8), 8.

Levesque, M., Saurer, M., Siegwolf, R., Eilmann, B., Brang, P., Bugmann, H., Rigling, A., 2013. Drought response of five conifer species under contrasting water availability suggests high vulnerability of Norway spruce and European larch. Glob. Chang. Biol. 19, 3184–3199. https://doi.org/10.1111/gcb.12268.

Lewis, J.D., Lucash, M., Olszyk, D., Tingey, D.T., 2001. Seasonal patterns of photosynthesis in douglas fir seedlings during the third and fourth year of exposure to elevated CO2 and temperature. Plant Cell Environ. 24, 539–548. https://doi.org/10.1046/j.1365-3040.2001.00700.x.

Littell, J.S., Peterson, D.L., Tjoelker, M., 2008. Douglas-fir growth in mountain ecosystems: Water limits tree growth from stand to region. Ecol. Monogr. 78, 349–368. https://doi.org/10.1890/07-0712.1.

Little, R.L., Peterson, D.L., Silsbee, D.G., S, L.J., Bednar, L.F., 1995. Radial growth patterns and the effects of climate on second-growth Douglas-fir (Pseudotsuga menziesii) in the Siskiyou Mountains, Oregon. Can. J. Fish. Aquat. Sci. 25, 724–735.

Livingston, N.J., Spittlehouse, D.L., 1996. Carbon isotope fractionation in tree ring early and late wood in relation to intra-growing season water balance. Plant Cell Environ. 19, 768–774. https://doi.org/10.1111/j.1365-3040.1996.tb00413.x.

Lo, Y.H., Blanco, J.A., Seely, B., Welham, C., Kimmins, J.P. (Hamish), 2010. Relationships between climate and tree radial growth in interior British Columbia, Canada. For. Ecol. Manage. 259, 932–942. https://doi.org/10.1016/j.foreco.2009.11.033.

Martinez-Meier, A., Sanchez, L., Pastorino, M., Gallo, L., Rozenberg, P., 2008. What is hot in tree rings? The wood density of surviving Douglas-firs to the 2003 drought and heat wave. For. Ecol. Manage. 256, 837–843. https://doi.org/10.1016/j.foreco.2008.05.041.

McCarroll, D., Loader, N.J., 2004. Stable isotopes in tree rings. Quat. Sci. Rev. 23, 771–801. https://doi.org/10.1016/j.quascirev.2003.06.017.

McNulty, S.G., Swank, W.T., 1995. Wood (delta)^(13)C as a measure of annual basal area growth and soil water stress in a *Pinus strobus* forest. Ecology 76, 1581–1586. https://doi.org/10.2307/1938159.

Novick, K.A., Ficklin, D.L., Stoy, P.C., Williams, C.A., Bohrer, G., Oishi, A.C., Papuga, S.A., Blanken, P.D., Noormets, A., Sulman, B.N., Scott, R.L., Wang, L., Phillips, R.P., 2016. The increasing importance of atmospheric demand for ecosystem water and carbon fluxes. Nat. Clim. Chang. 6, 1023–1027. https://doi.org/10.1038/nclimate3114.

Pinheiro, J., D. Bates, R Core Team, 2022._nlme: Linear and Nonlinear Mixed Effects Models_.

Restaino, C.M., Peterson, D.L., Littell, J., 2016. Increased water deficit decreases Douglas fir growth throughout western US forests. Proceedings of the National Academy of Sciences of the United States of America 113, 9557–9562. https://doi.org/10.1073/pnas.1602384113.

Rinne, K.T., Boettger, T., Loader, N.J., Robertson, I., Switsur, V.R., Waterhouse, J.S., 2005. On the purification of α-cellulose from resinous wood for stable isotope (H, C and O) analysis. Chem. Geol. 222, 75–82. https://doi.org/10.1016/j.chemgeo.2005.06.010.

Robertson, E.O., Jozsa, L.A., Spittlehouse, D.L., 1990. Estimating Douglas-fir wood production from soil and climate data. Can. J. For. Res. 20, 357–364.

Rubio-Cuadrado, Á., Camarero, J.J., Bosela, M., 2022. Applying climwin to dendrochronology: A breakthrough in the analyses of tree responses to environmental variability. Dendrochronologia 71, 125916. https://doi.org/10.1016/j.dendro.2021.125916.

Ruehr, N.K., Law, B.E., Quandt, D., Williams, M., 2014. Effects of heat and drought on carbon and water dynamics in a regenerating semi-arid pine forest: A combined experimental and modeling approach. Biogeosciences 11, 4139–4156. https://doi.org/10.5194/bg-11-4139-2014.

Sanginés de Cárcer, P., Vitasse, Y., Peñuelas, J., Jassey, V.E.J., Buttler, A., Signarbieux, C., 2018. Vapor–pressure deficit and extreme climatic variables limit tree growth. Glob. Chang. Biol. 24, 1108–1122. https://doi.org/10.1111/gcb.13973.

Spies, T., 2016. LiDAR data (October 2011) for the Upper Blue River Watershed, Willamette National Forest. Long-Term Ecological Research. Forest Science Data Bank, Corvallis, OR. [Database]. Available: http://andlter.forestry.oregonstate.edu/data/abstract.aspx?dbcode=GI011. https://doi.org/10.6073/pasta/8e4f57bafaaad5677977dee51bb3077c. Accessed 2023-03-09.

Sulman, B.N., Roman, D.T., Yi, K., Wang, L., Phillips, R.P., Novick, K.A., 2016. High atmospheric demand for water can limit forest carbon uptake and transpiration as severely as dry soil. Geophys. Res. Lett. 9686–9695 https://doi.org/10.1002/2016GL069416.Received.

Swanson, F.J., James, M.E., 1975. Geology and geomorphology of the H.J. Andrews Experimental Forest, Western Cascades, Oregon, Pac. Northwest Forrest and Range Experiment Station, Forest Service, U.S. Dept. of Agriculture. Portland, OR.

van de Pol, M., Baily, L.D., McLean, N., Rijsdijk, L., Lawson, C.R., Brouwer, L., 2016. Identifying the best climatic predictors in ecology and evolution Methods in Ecology and Evolution.

Williams, A.P., Allen, C.D., Millar, C.I., Swetnam, T.W., Michaelsen, J., Still, C.J., Leavitt, S.W., 2010. Forest responses to increasing aridity and warmth in the southwestern United States. PNAS 107, 21289–21294. https://doi.org/10.1073/pnas.0914211107.

Williams, P.A., Allen, C.D., Macalady, A.K., Griffin, D., Woodhouse, C.A., Meko, D.M., Swetnam, T.W., Rauscher, S.A., Seager, R., Grissino-Mayer, H.D., Dean, J.S., Cook, E.R., Gangodagamage, C., Cai, M., Mcdowell, N.G., 2013. Temperature as a potent driver of regional forest drought stress and tree mortality. Nat. Clim. Chang. 3, 292–297. https://doi.org/10.1038/nclimate1693.

Yuan, W., Zheng, Y., Piao, S., Ciais, P., Lombardozzi, D., 2019. Increased atmospheric vapor pressure deficit reduces global vegetation growth. Sci. Adv. 1–13.

Zhang, Q., Alfaro, R.I., Hebda, R.J., 1999. Dendroecological studies of tree growth, climate and spruce beetle outbreaks in Central British Columbia, Canada. For. Ecol. Manage. 121, 215–225. https://doi.org/10.1016/S0378-1127(98)00552-0.

Zhang, Q., Hebda, R.J., 2004. Variation in radial growth patterns of Pseudotsuga menziesii on the central coast of British Columbia, Canada. Can. J. For. Res. 34, 1946–1954. https://doi.org/10.1139/X04-078.

Zweifel, R., Sterck, F., Braun, S., Buchmann, N., Eugster, W., Gessler, A., Häni, M., Peters, R.L., Walthert, L., Wilhelm, M., Ziemińska, K., Etzold, S., 2021. Why trees grow at night. New Phytol. 231, 2174–2185. https://doi.org/10.1111/nph.17552.